Similarity solutions for van der Waals rupture of a thin film on a solid substrate

Wendy W. Zhang
Division of Engineering and Applied Sciences, Harvard University, Cambridge, Massachusetts 02138

John R. Lister
Institute of Theoretical Geophysics, DAMTP, University of Cambridge, Cambridge CB3 9EW, United Kingdom

(Received 29 December 1998; accepted 26 May 1999)

Rupture of a thin viscous film on a solid substrate under a balance of destabilizing van der Waals pressure and stabilizing capillary pressure is shown to possess a countably infinite number of similarity solutions in each of which the horizontal lengthscale decreases like $(t_R-t)^{2/5}$ and the film thickness decreases like $(t_R-t)^{1/5}$, where t_R-t is the time remaining before rupture. Only the self-similar solution corresponding to the least oscillatory curvature profile is observed in time-dependent numerical simulations of the governing partial differential equation. The numerical strategy employed to obtain the self-similar solutions is developed from far-field asymptotic analysis of the similarity equations. © *1999 American Institute of Physics.* [S1070-6631(99)03509-6]

I. INTRODUCTION

Van der Waals forces can cause a thin liquid film on a solid substrate to rupture and form a dry spot despite the stabilizing influence of surface tension. Liquid-film rupture on a substrate is an important, if sometimes undesirable, phenomenon in a variety of coating, drying, and cooling problems. Van-der-Waals-driven film rupture is an important step in the collapse of a foam and in droplet coalescence. In each of these cases, accurate numerical simulation through the topological singularity of rupture is aided by knowledge of the way the singularity is approached.

Film rupture on a solid substrate provides one example of a general class of finite-time free-surface singularity problems that have received much attention recently. Other examples are the breakup of a thin liquid thread by surface tension,[1–6] the rupture of a thin freely suspended liquid sheet by van der Waals forces,[7,8] and topology changes in a Hele–Shaw cell.[9–12] In all these problems the dynamics close in space and time to the singularity are solely determined by the approach to singularity and therefore can be described by self-similar solutions that are independent of far-field and initial conditions. This independence greatly simplifies numerical modeling as it allows investigators to draw general conclusions about the structure of the singularity from observations of the evolution of the system towards a singularity from one particular set of boundary and initial conditions.

The problem studied in this paper falls within a class of problems with governing equations of the form

$$\frac{\partial h}{\partial t} = A\nabla\cdot(h^m\nabla h) - B\nabla\cdot(h^n\nabla\nabla^2 h). \tag{1}$$

The case $B=0$ is the well-known nonlinear diffusion equation, for which similarity solutions have been known for many years (e.g., Ref. 13). More recently, the case $A=0$ has been the subject of an extensive series of studies both as a model equation for surface-tension-driven flows and from a mathematical viewpoint.[14–16] The combination of the two terms on the right-hand side of (1) has been considered by Bertozzi and Pugh,[17,18] who proved a number of mathematical results concerning boundedness, blowup, the existence of weak solutions with compact support, and traveling-wave solutions for ''moving contact lines,'' but did not construct similarity solutions for pinching singularities. Pinching singularities have been analyzed for the case $m=n=1$ which describes the Rayleigh–Taylor problem in a Hele–Shaw cell,[11] and for an equation comparable to the case $m=0$, $n=-2$, but with modifications to account for geometry, which occurs in axisymmetric surface diffusion.[19,20]

The physical problem of thin-film evolution under surface tension and van der Waals forces is described by (1) with $m=3$, $n=-1$, as derived by Williams and Davis[21] and many other authors. In this paper we are concerned with pinching singularities of (1) corresponding to film rupture. From numerical simulations of two-dimensional van der Waals rupture of a thin liquid film on a solid substrate, Burelbach *et al.*,[22] proposed that the effect of surface tension becomes negligible near rupture so that the asymptotic self-similar behavior is determined only by a balance of van der Waals forces and viscous dissipation. An analytic solution for this balance and consistent with the neglect of surface tension is given in a recent review.[23] We present a reanalysis of the problem in both two-dimensional and axisymmetric geometries and show by time-dependent numerical simulations of the governing partial differential equations that the effects of surface tension are not asymptotically negligible. Indeed, the requirement that surface tension, van der Waals forces, and viscous dissipation are equally important near rupture fully determines the scalings of the horizontal and vertical lengthscales. In both geometries the partial differen-

tial equations describing rupture admit a countably infinite family of similarity solutions and the solution observed in the time-dependent simulations of the partial differential equation corresponds to the similarity solution with the least oscillatory curvature profile near the origin.

The paper is organized as follows: in the next section we sketch the derivation of the fourth-order nonlinear diffusion equation which describes the evolution of the film thickness. In Sec. III we present results from numerical simulations of axisymmetric film rupture. The form of the similarity solution is deduced from the results of the numerical simulations and then used to derive an ordinary differential equation for the self-similar film thickness from the governing time-dependent equations. In Sec. IV we present analysis and solutions for the similarity ordinary differential equation associated with axisymmetric rupture. The similarity problem poses some interesting challenges for numerical solution, owing to nonlinearities and to the large number of derivatives in the problem, which combine to give rise to oscillations in the film thickness and to a variety of far-field asymptotic behaviors. In Sec. V we present time-dependent numerical simulations and similarity solutions for a two-dimensional geometry. Results from the time-dependent simulations in both axisymmetric and two-dimensional geometries agree well with the similarity solution that possesses the least oscillatory curvature profile. In Sec. VI we conclude by establishing the limits of validity for the self-similar regime found in Secs. III–V. Details of the numerical schemes used in the time-dependent simulations are given in the Appendix.

II. PROBLEM FORMULATION

Consider a nonwetting fluid layer with initial thickness h_0. Owing to the destabilizing effects of van der Waals forces, small disturbances of the film thickness can grow and cause the film to rupture. We follow previous studies by assuming that the initial destabilizing disturbances are long wavelength and therefore the rupture process, at least in its early stages, can be described by the usual lubrication approximation to the Navier–Stokes equations. Let z be the coordinate normal to the flat solid substrate underlying the film, and $\mathbf{x}_H$, $\mathbf{u}_H$, and ∂_H be the components of displacement, velocity, and gradient vectors parallel to the substrate. For typical fluids, gravity is negligible on lengthscales for which van der Waals forces are significant. The governing equations then take the form

$$0 = -\nabla_H p + \mu \frac{\partial^2 \mathbf{u}_H}{\partial z^2}, \tag{2}$$

$$0 = -\frac{\partial p}{\partial z}, \tag{3}$$

$$\frac{\partial h}{\partial t} + \nabla_H \cdot \int_0^h \mathbf{u}_H \, dz = 0, \tag{4}$$

where μ denotes the fluid viscosity and $h(\mathbf{x}_H, t)$ the film thickness. The collective effect of van der Waals attractions between molecules in the fluid film and those in the solid substrate and in the air above can be described as a macroscopic body force and incorporated into a modified pressure.[24] The fluid pressure p in (3) thus contains a contribution from van der Waals forces in addition to the usual contribution from surface tension. For a sufficiently thin and nearly flat film, we write

$$p(\mathbf{x}_H, t) = \frac{A^*}{6\pi h^3} - \gamma \nabla_H^2 h, \tag{5}$$

where γ is the coefficient of surface tension and A^* is the Hamaker constant, which reflects the strength of the various intermolecular attractions.

Imposing a no-slip condition at the solid substrate and a free-slip condition at the film surface in (2), we obtain from (2), (4), and (5) that

$$\frac{\partial h}{\partial t} + \nabla_H \cdot \left[\frac{h^3}{3\mu} \nabla_H \left(\gamma \nabla_H^2 h - \frac{A^*}{6\pi h^3} \right) \right] = 0. \tag{6}$$

Equation (6) is the fourth-order nonlinear diffusion equation describing the evolution of the film thickness. The two-dimensional version of (6) was that studied by Burelbach *et al.*[22]

Dimensional analysis of (6), as well as more detailed stability studies,[21] suggests that a flat film of initial thickness h_0 is linearly unstable to sinusoidal perturbations whose wavelengths are greater than or comparable to h_0^2/d^*, where

$$d^* = (A^*/\gamma)^{1/2} \tag{7}$$

is the molecular lengthscale. For a continuum approach to be valid, we require $h_0 \gg d^*$, which implies that $h_0^2/d^* \gg h_0$ and hence that the initial instability has a long wavelength, in agreement with our original assumption.

As the film thins towards rupture, the characteristic length- and timescales of the problem change by orders of magnitude so that (6) cannot be nondimensionalized by these scales. Instead h, $\mathbf{x}_H$, and t are nondimensionalized in a way that recasts (6) in a form independent of the material parameters. One such nondimensionalization uses a characteristic film thickness $\hat{h}$, lateral lengthscale $\hat{l}$, and timescale $\hat{t}$ defined by

$$\hat{h} = h_0, \tag{8a}$$

$$\hat{l} = \frac{h_0^2}{d^*}, \tag{8b}$$

$$\hat{t} = \frac{12\pi^2 \mu \gamma h_0^5}{A^{*2}}; \tag{8c}$$

another uses an arbitrary lengthscale in place of h_0 in (8a)–(8c). From now on all variables will be nondimensional unless stated otherwise.

III. AXISYMMETRIC TIME-DEPENDENT SIMULATIONS

Numerical simulation of axisymmetric free-surface evolution proceeded from the nondimensional form of (6),

$$\frac{\partial h}{\partial t} + \frac{1}{r}\frac{\partial}{\partial r}\left[r h^3 \frac{\partial}{\partial r}\left(\frac{1}{r}\frac{\partial}{\partial r}\left(r \frac{\partial h}{\partial r} \right) \right) + \frac{r}{h}\frac{\partial h}{\partial r} \right] = 0, \tag{9}$$

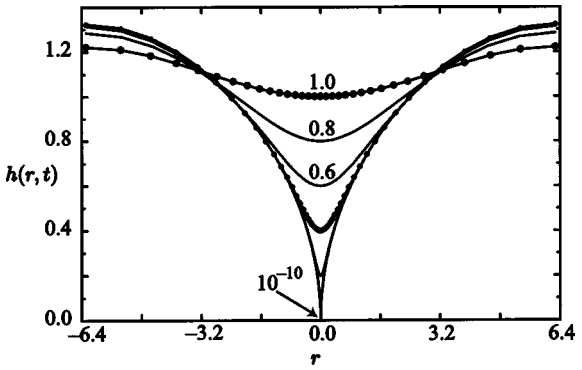

FIG. 1. Film profiles $h(r,t)$ at $h_{\min}(t)=1.0$, 0.8, 0.6, 0.4, 0.2, and 10^{-10}. Circles placed on profiles at $h_{\min}(t)=1.0$ and $h_{\min}(t)=0.4$ correspond to points used in the time-dependent simulation.

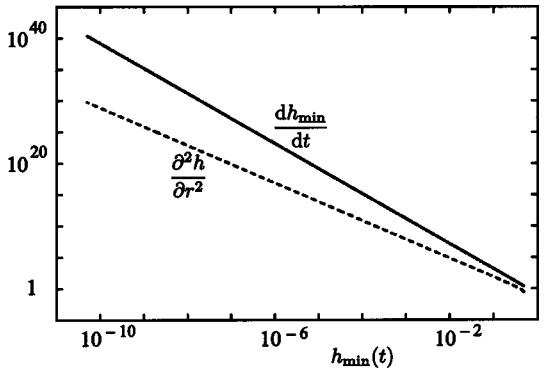

FIG. 2. $dh_{\min}/dt$ (solid line) and $\partial^2 h/\partial r^2$ (dashed line) versus $h_{\min}(t)$. After a short transient, the solid line has slope -4 and the dashed line has slope -3. The intercepts can be used to infer $H(0)$ and $H''(0)$ in the similarity form (11).

where r is the radial coordinate. The numerical scheme used finite differences with implicit representation of the highest spatial derivatives. To resolve the self-similar behavior close to rupture, we used an adaptive variable-grid scheme which maintains a roughly constant number of grid points over a horizontal length comparable with the square of the current minimum film thickness, a choice which is consistent with the anticipated self-similar scaling. The size of the time step was then chosen to be consistent with the desired spatial resolution.

The initial free-surface profile was taken to be

$$h(r,0)=\frac{10}{9}\left[1-\frac{1}{10}\cos\left(\frac{2\pi r}{\lambda}\right)\right], \tag{10}$$

which is qualitatively similar to a linear axisymmetric perturbation mode of the thin film. Equation (9) was solved on the fixed interval $0\leqslant r\leqslant\lambda/4$ and the wavelength λ was chosen to be sufficiently long for linear instability. Boundary conditions $\partial h/\partial r=\partial^3 h/\partial r^3=0$ were imposed at $r=0$ and $r=\lambda/4$. The conditions at $r=0$ are required for the solution to be regular at that point; the initial condition and the boundary conditions at $r=\lambda/4$ were simply chosen for convenience, and the behavior close to the rupture does not depend on this choice. The simulation began with minimum film thickness $h_{\min}(t=0)=1$ and proceeded through ten decades until $h_{\min}(t)=10^{-10}$. More details about the numerical scheme can be found in the Appendix.

A few snapshots of the film profile toward the beginning of the simulation are shown in Fig. 1, along with the film profile reached at the end of the run. To illustrate the adaptive, variable-grid scheme used in the simulation, grid points are shown on top of the film profiles at $h_{\min}(0)=1$ and $h_{\min}(t)=0.4$. It may be noted that rupture occurs at the center point $r=0$, and fluid is not trapped in a dimple as can occur when two drops approach each other without van der Waals attractions.[25]

The plot of $dh_{\min}/dt$ and $\partial^2 h/\partial r^2(0)$ versus $h_{\min}(t)$ in Fig. 2 suggests that the minimum film thickness varies as $(t_R-t)^{1/5}$, where t_R is the time of rupture, while the characteristic horizontal lengthscale varies as $h_{\min}^2(t)$. A test of the scalings suggested by these variations is provided by Fig. 3, which plots the rescaled second derivative $h_{\min}^3\partial^2 h/\partial r^2$ as a function of the rescaled radial distance $r/h_{\min}^2$ at successive times. The rapid convergence of $h_{\min}^3\partial^2 h/\partial r^2$ to a fixed shape confirms that (9) has a similarity solution of the form

$$h(r,t)=(t_R-t)^{1/5}H(\eta), \quad \eta=\frac{r}{(t_R-t)^{2/5}}. \tag{11}$$

For later comparisons with solutions to the similarity ordinary differential equations, we note that fitting power laws to the results in Fig. 2 gives $H(0)=0.7681$ and $H''(0)=0.1687$. We also note for later discussion that the time dependence shown in (11) implies that the long-wavelength approximation must eventually fail.

A plot of the rescaled film thickness $h(r,t)/h_{\min}(t)$ at $h_{\min}=10^{-10}$ (Fig. 4) shows that, on the intermediate range of lengthscales $h_{\min}^2(t)\ll r\ll\lambda/4$, the film thickness varies approximately as $Ar^{1/2}$, where $A=0.6763$. We can see from (11) that this intermediate behavior corresponds to a quasi-steady far field in the similarity solution. The film thickness deviates from the intermediate scaling when $r=O(1)$ in order to accommodate the imposed boundary conditions.

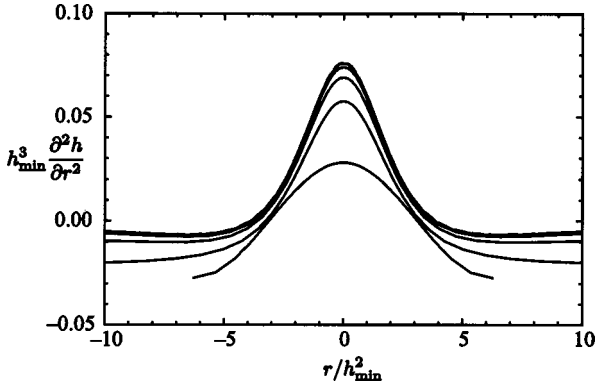

FIG. 3. Rescaled second derivative $h_{\min}^3\partial^2 h/\partial r^2$ versus rescaled radial distance $r/h_{\min}^2$. Solid curves correspond to profiles at $h_{\min}=1.0$, 0.8, 0.6, 0.4, and 0.2; the dashed curve corresponds to the profile at $h_{\min}=10^{-10}$. Rapid convergence to a self-similar profile is almost complete by $h_{\min}=0.2$.

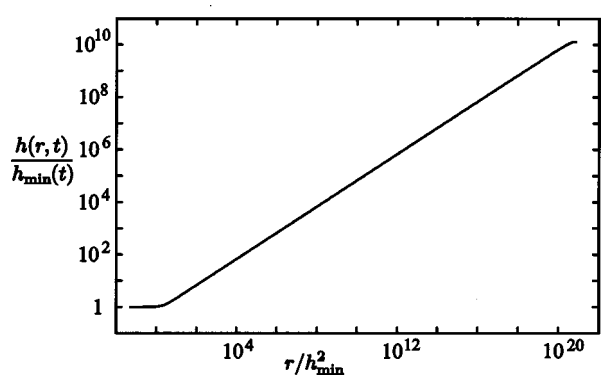

FIG. 4. Rescaled film profile $h(r,t)/h_{\min}(t)$ versus rescaled radial distance $r/h_{\min}^2$. Note the $r^{1/2}$ dependence extending over the range of lengthscales intermediate between the $r=O(h_{\min}^2)$ region of rupture and the $r=O(1)$ size of the domain.

IV. AXISYMMETRIC SIMILARITY SOLUTIONS

Substitution of the similarity ansatz (11) into the governing equation (9) yields an ordinary differential equation for self-similar axisymmetric rupture,

$$\frac{1}{5}(H-2\eta H')=\frac{1}{\eta}\left[\frac{\eta H'}{H}+\eta H^3\left(\frac{(\eta H')'}{\eta}\right)'\right]', \tag{12}$$

where $'$ denotes differentiation with respect to the similarity variable η. Two boundary conditions, $H'(0)=H'''(0)=0$, are imposed at the origin for regularity. The values of $H(0)$ and $H''(0)$ are determined by shooting for boundary conditions at infinity.

A. Far-field asymptotic behavior

Since the self-similar behavior of locally driven rupture should be asymptotically insensitive to the boundary conditions imposed at the end of the unscaled interval, the far-field boundary condition for the similarity solution is that of quasi-steady behavior: the quasi-steady condition $\partial h/\partial t \ll h/t$ far from rupture in (9) translates into the boundary condition $\frac{1}{5}(H-2\eta H')\ll H$ or, equivalently, $H\sim A\eta^{1/2}$ as $\eta\to\infty$ in (12). In fact,

$$H_{1/2}(\eta)=A\eta^{1/2} \tag{13}$$

is an exact solution of (12) for all values of the constant A.

Since (13) has only one free constant, it is not immediately clear that requiring $H\sim A\eta^{1/2}$ imposes the correct number of boundary conditions at infinity or that it allows matching to the boundary conditions at the origin. However, linearizing (12) about (13) by writing $H=H_{1/2}+\Delta H_{1/2}$ reveals that the asymptotic form (13) has one perturbation mode which corresponds to a small change in the value of A and three exponential perturbation modes of the form

$$\Delta H_{1/2}=a_0\eta^{-1}e^{\chi_0(\eta)}+a_+\eta^{-1}e^{\chi_+(\eta)}+a_-\eta^{-1}e^{\chi_-(\eta)}, \tag{14}$$

where

$$\chi_0(\eta)\sim-\frac{\beta\eta^{5/6}}{A},\quad \chi_\pm(\eta)\sim\frac{e^{\pm i\pi/3}\beta\eta^{5/6}}{A},$$

$$\beta=\frac{6}{5}\left(\frac{2}{5}\right)^{1/3}. \tag{15}$$

Thus the requirement that $H(\eta)\sim A\eta^{1/2}$ is equivalent to the requirement that the amplitudes $a_\pm$ of the two growing modes must vanish as $\eta\to\infty$, which constitutes two boundary conditions. We therefore expect, and indeed will find, that the desired similarity solutions exist at isolated points in the $(H(0),H''(0))$ parameter plane.

Before proceeding to a numerical search for the desired similarity solutions of (12), it is helpful to note what alternative far-field behavior is produced by (12) in the remainder of the $(H(0),H''(0))$ plane. One alternative requires

$$\left[\eta H^3\left(\frac{(\eta H')'}{\eta}\right)'\right]'\sim 0 \quad \text{as} \quad \eta\to\infty \tag{16}$$

and yields

$$H_2(\eta)\sim C\eta^2+\frac{3}{80C^2}(\ln\eta)^2+D\ln\eta, \tag{17}$$

where C and D are free constants. Linear perturbation analysis indicates that the η^2 far-field behavior is always structurally stable and therefore constitutes the generic behavior in the $(H(0),H''(0))$ plane. The other alternative requires

$$\frac{1}{5}(H-2\eta H')\sim\frac{1}{\eta}\left[\eta H^3\left(\frac{(\eta H')'}{\eta}\right)'\right]' \quad \text{as} \quad \eta\to\infty, \tag{18}$$

and yields the far-field asymptotic behavior $H(\eta)\sim H_{4/3}(\eta)$, where

$$H_{4/3}(\eta)=B_p\eta^{4/3},\quad B_p=\left(\tfrac{27}{320}\right)^{1/3} \tag{19}$$

is also an exact solution. The four linear perturbation modes about (19) have the form η^m, where $27m^4+144m^3+180m^2-320=0$. One of the four roots gives a growing mode, so that requiring $H\sim\eta^{4/3}$ constitutes one boundary condition at infinity. Thus this kind of solution occurs at parameter values which lie on curves in the $(H(0),H''(0))$ plane. For ease of reference, we shall refer to a solution with $H\sim\eta^{1/2}$ asymptotic behavior as an $\eta^{1/2}$ solution, a solution with $H\sim\eta^{4/3}$ asymptotic behavior as an $\eta^{4/3}$ solution and the generic solution (17) as an η^2 solution.

The numerical problem is now seen to be that of finding the isolated values of $H(0)$ and $H''(0)$ that give the asymptotic far-field behavior (13) as $\eta\to\infty$ in a plane of values that almost always give rise to the asymptotic far-field behavior of (17) or (19). The simple strategy of first zeroing the coefficient C of the largest asymptotic term in the η^2 solution, and then zeroing the coefficient B_p of the next largest term in the $\eta^{4/3}$ solution, fails since B_p is a fixed number and not a free coefficient. The problem is complicated by the fact that, as in many capillary problems, (12) supports solutions with oscillations and hence the far-field behavior is not a monotonic function of the shooting parameter. The following sections describe two numerical strategies devised to overcome these complications.

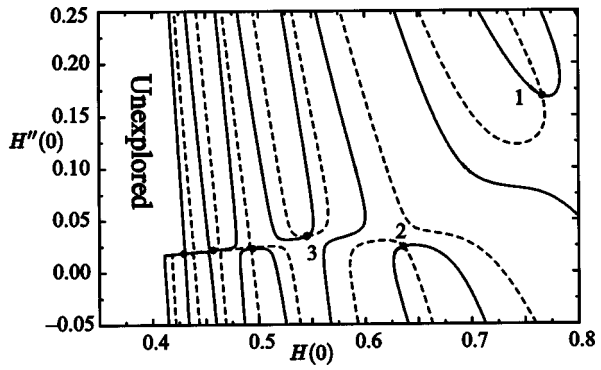

FIG. 5. Results of the search for solutions with $\eta^{1/2}$ far-field behavior. Solid and dashed curves correspond to solutions satisfying the $H-2\eta H'=0$ and $H+4\eta^2H''=0$ end conditions at $\eta=10$. Dots correspond to solutions with the desired $\eta^{1/2}$ far-field behavior.

B. $\eta^{1/2}$ solutions

The desired $\eta^{1/2}$ solutions were first obtained by a numerical shooting scheme in which (12) was integrated using a fourth-order Runge–Kutta scheme from the origin to some large value of η, which ranged from 10 to 200. Estimates of the shooting parameters $H(0)$ and $H''(0)$ were used to start the integration. These parameters were adjusted so that

$$H-2\eta H'=0 \quad \text{and} \quad H+4\eta^2H''=0 \tag{20}$$

at the end of the integration range—the two end conditions (20) were chosen to be independent, to involve low-order derivatives and to together require $H(\eta)\propto\eta^{1/2}$ at the end of the integration interval; other choices are certainly possible. To avoid the coordinate singularity at the origin, a five-term Taylor series was used to start the numerical integration at $\eta=10^{-4}$. The distance 10^{-4} was chosen to be at most $\frac{1}{20}$ of the radius of convergence for $H(0)$ and $H''(0)$ in the region of interest in parameter space. The local radius of convergence was estimated from the decay of the first 200 Taylor series coefficients; it varies strongly with $H(0)$ and only weakly with $H''(0)$.

Results of this preliminary search for $\eta^{1/2}$ solutions are illustrated in Fig. 5, where the solid curves correspond to values of $(H(0),H''(0))$ which satisfy the end condition $H-2\eta H'=0$ while the dashed curves correspond to values of $(H(0),H''(0))$ that satisfy the end condition $H+4\eta^2H''=0$. Dots at the intersections of the two sets of curves correspond to $\eta^{1/2}$ solutions. Since neither end condition alone is sufficient to locate a $\eta^{1/2}$ solution, points on only one of the solid and dashed curves have little significance in themselves and correspond to solutions with η^2 or $\eta^{4/3}$ far-field behavior if the integration range is extended to infinity. Experimentation with different integration intervals showed that as the integration interval is extended, the shapes of the curves change significantly but the locations of the intersections remain essentially unchanged. The spacing between intersections decreases in the parameter limit $H(0)\to 0$, $H''(0)\to 0$, which suggests that (12) has a countably infinite number of $\eta^{1/2}$ similarity solutions.

The results of the preliminary search described above were then refined by a search scheme described in the next section, which makes use of the way $\eta^{1/2}$ and $\eta^{4/3}$ solutions are related in this problem. Here we restrict ourselves to some comments on the values of $H(0)$, $H''(0)$, and A associated with the first six similarity solutions given in Table I. Though the numerical values are dependent on the scaling used to derive (9), their relative spacing is not. The coefficient A of the $\eta^{1/2}$ far-field behavior decreases monotonically with $H(0)$ while the curvature at the origin $H''(0)$ decreases in an oscillatory fashion.

TABLE I. Various quantities associated with the first six similarity solutions for axisymmetric rupture. Self-similar dynamics deduced from time-dependent axisymmetric simulations yield values $H(0)=0.7681$, $H''(0)=0.1687$, and $A=0.6763$, which are consistent with the first similarity solution.

$H(0)$	$H''(0)$	A
0.768 178 509 6	0.168 731 448 2	0.676 32
0.637 424 688	0.024 570 167 5	0.452 93
0.546 865 550 8	0.034 961 263 4	0.375 148
0.495 583 051	0.023 138 214 6	0.329 95
0.458 624 50	0.021 649 009	0.299 22
0.430 800	0.018 417 65	0.276 430

In Fig. 6 we have plotted $H(\eta)$ and $H'''(\eta)$ for the first, third, and fifth similarity solutions, together with the self-similar profiles observed in the time-dependent simulation. The self-similar dynamics observed in the time-dependent simulations of (9) closely corresponds to the first similarity solution of (12). None of the higher-order similarity solu-

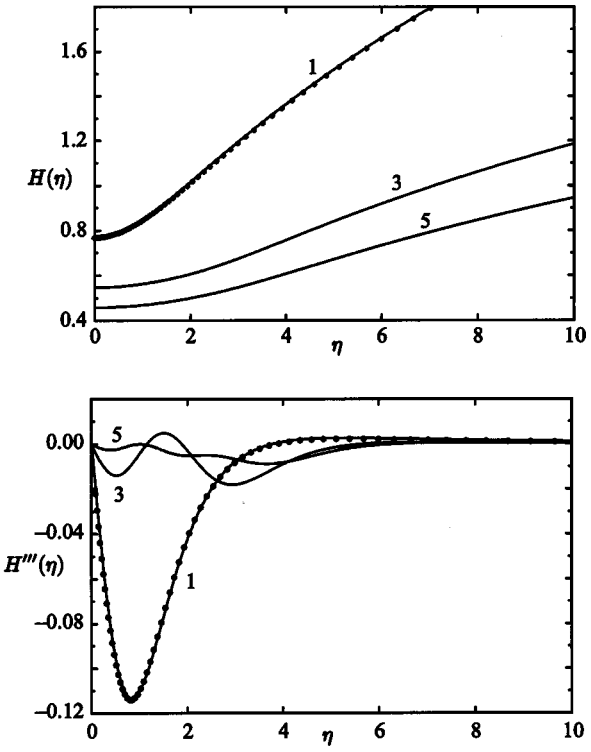

FIG. 6. Plots of $H(\eta)$ and $H'''(\eta)$ for the first, third, and fifth axisymmetric similarity solutions (lines) together with results from the time-dependent simulations (circles). Successive similarity solutions have an extra half-oscillation in $H'''(\eta)$.

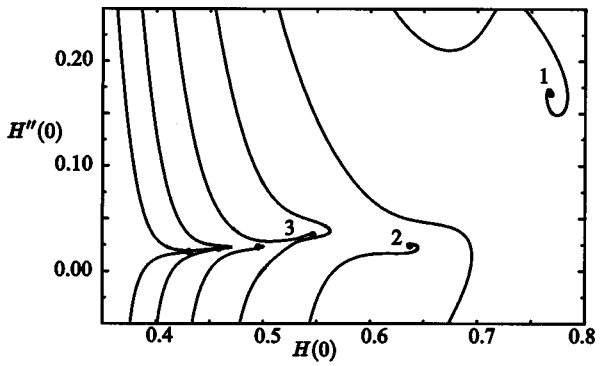

FIG. 7. Results of the search for solutions with $B_p\eta^{4/3}$ far-field asymptotic behavior. Solid curves correspond to these solutions; dots correspond to solutions with the desired $\eta^{1/2}$ far-field behavior. The numerical integration range is $\eta=50$.

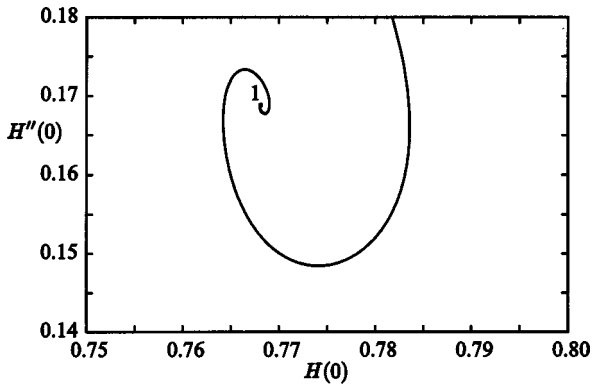

FIG. 8. A closeup of the spiraling end of the $\eta^{4/3}$ parameter curve associated with the first axisymmetric similarity solution.

tions has been observed in time-dependent simulations, which suggests that they are unstable. (This has since been confirmed by a stability analysis.[25])

A comparison of $H'''(\eta)$ profiles shows that the similarity solutions are ordered by structure as well as by $H(0)$: as $H(0)$ decreases, each successive similarity solution experiences an extra half-oscillation before asymptoting towards the $\eta^{1/2}$ far-field behavior. This ordering by structure allows us to deduce that there are no similarity solutions at larger values of $H(0)$. Hence we conclude that the self-similar solution observed in time-dependent simulations is the one with the least oscillatory curvature profile.

C. $\eta^{4/3}$ solutions

Having located the points corresponding to $\eta^{1/2}$ solutions in the $(H(0),H''(0))$ plane, we considered their relation to the more generic η^2 and $\eta^{4/3}$ solutions. To do so we solved (12) for the one-parameter family of curves corresponding to the $\eta^{4/3}$ solutions. The same numerical shooting scheme was employed, except that the end condition was now chosen to be $H-(9/4)\eta^2H''=0$. Of all the curves obtained this way, only those with $H'''<0$ at the end correspond to $\eta^{4/3}$ solutions as the integration range is extended towards infinity; those with $H'''>0$ correspond to transients before eventual η^2 far-field behavior and were discarded.

Results of the search for $\eta^{4/3}$ solutions are illustrated in Fig. 7. Some $\eta^{4/3}$ parameter curves run smoothly from $+\infty$ to $-\infty$, but others appear to terminate in a spiral about values of $(H(0),H''(0))$ which yield $\eta^{1/2}$ solutions. These observations are confirmed by the asymptotic behavior of terminating $\eta^{4/3}$ parameter curves as the integration range is extended. We have also plotted profiles of $H(\eta)$ for points along the $\eta^{4/3}$ parameter curve and observed that, as $(H(0),H''(0))$ approach the end of the spiral, the $H(\eta)$ profile develops a lengthening $\eta^{1/2}$ transient. Indeed, we found that locating $\eta^{1/2}$ solutions by finding the terminations of the $\eta^{4/3}$ spirals was a more robust strategy than finding roots of (20), since there is less variation of the curves in the parameter plane as the integration range is extended towards infinity. Hence rough estimates of the parameter values corresponding to $\eta^{1/2}$ solutions obtained from our preliminary search were refined by locating the termination points of the $\eta^{4/3}$ spirals. A plot of the spiral corresponding to the first similarity solution is given in Fig. 8.

Some explanation for the existence of a spiral of $\eta^{4/3}$ solutions around an $\eta^{1/2}$ solution is provided by (14) and (15): the two growing perturbation modes around an $\eta^{1/2}$ solution are oscillatory, and their initially small amplitudes are linearly related to the deviation of $H(0)$ and $H''(0)$ from the values that give a true $\eta^{1/2}$ solution. If the phase of these modes is right when their amplitudes and nonlinear interactions have grown to $O(1)$, then an $\eta^{4/3}$ solution results.

V. TWO-DIMENSIONAL TIME-DEPENDENT SIMULATIONS

A two-dimensional rupture process is described by

$$\frac{\partial h}{\partial t}+\frac{\partial}{\partial x}\left[\left(h^3\frac{\partial^3 h}{\partial x^3}+\frac{1}{h}\frac{\partial h}{\partial x}\right)\right]=0 \tag{21}$$

with the initial condition (10) and symmetry boundary conditions $\partial h/\partial x=\partial^3 h/\partial x^3=0$ at the origin and at the end of the interval. An adaptive, variable-grid scheme, similar to the one used in the axisymmetric time-dependent simulation, was employed to solve (21). The two-dimensional simulations give results which, when plotted in an analogous manner to Figs. 2–4, show clear asymptotic self-similarity. The similarity scaling is given by (11) with r replaced by x, and the numerical results yield $H(0)=0.7326$, $H''(0)=0.3007$, and $A=0.8068$.

The similarity ansatz (11) reduces the time-dependent problem (21) to the ordinary differential equation

$$\frac{1}{5}(H-2\eta H')=\left(\frac{H'}{H}+H^3H'''\right)', \tag{22}$$

with symmetry boundary conditions $H'(\eta)=H'''(\eta)=0$ at the origin and quasi-steady boundary conditions at infinity.

As in the axisymmetric rupture problem, (22) admits three types of solutions which vary, respectively, like η^2, $\eta^{4/3}$, and $\eta^{1/2}$ as $\eta\to\infty$. Each solution corresponds to the same balance of terms in (22) as the axisymmetric case and has the same number of growing perturbation modes. However, unlike in the axisymmetric problem, $A\eta^{1/2}$ and $B_p\eta^{4/3}$

TABLE II. Various quantities associated with the first six similarity solutions for two-dimensional rupture. Self-similar dynamics deduced from time-dependent two-dimensional simulations yield $H(0)=0.7326$, $H''(0)=0.3007$, and $A=0.8068$, which are consistent with the first similarity solution.

$H(0)$	$H''(0)$	A
0.732 662 38	0.300 975 59	0.806 88
0.597 607 373	0.017 350 716	0.551 36
0.506 529 650	0.073 219 676	0.452 714
0.457 181 733 8	0.032 052 811 7	0.395 59
0.420 860 571 7	0.039 995 592	0.356 87
0.394 032 366 8	0.028 833 237	0.328 28

are not exact solutions of (22). The desired $\eta^{1/2}$ similarity solution can be shown to have the asymptotic form

$$H_{1/2}(\eta)=A\eta^{1/2}\left(1+\sum_{i=1}^{\infty}\frac{a_i}{(A\eta^{5/2})^i}\right), \tag{23}$$

where the coefficients a_i can be obtained once the free constant A is known. The $\eta^{4/3}$ solution has the asymptotic form

$$H_{4/3}(\eta)=B_p\eta^{4/3}\left(1+\sum_{i=1}^{\infty}\frac{b_i}{(B_p\eta^{10/3})^i}\right), \tag{24}$$

where $B_p=(27/56)^{1/3}$ and the coefficients b_i are also determined by (22). Numerical solution of (22) revealed the same type of behavior as for the axisymmetric problem: each of the desired $\eta^{1/2}$ similarity solutions occurs at a point in the $(H(0),H''(0))$ plane at which a parameter curve corresponding to the $\eta^{4/3}$ solution terminates, and there are a countably infinite number of such solutions. Table II lists the values of $H(0)$, $H''(0)$, and A associated with the first six $\eta^{1/2}$ similarity solutions for two-dimensional rupture. Figure 9 presents $H(\eta)$ and $H'''(\eta)$ for the first, third, and fifth similarity solutions of (22) along with the self-similar profiles from the time-dependent simulation. As in Fig. 6, the time-dependent result from (21) corresponds closely to the first similarity solution of (22). The similarity solutions of (22) exhibit the same intrinsic ordering: each successive $H'''(\eta)$ has an extra half-oscillation before asymptoting onto the far-field profile.

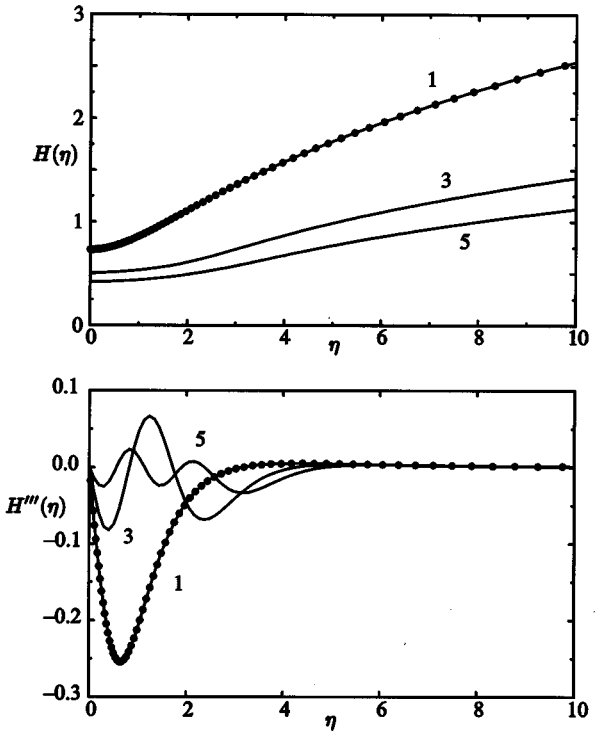

FIG. 9. Plots of $H(\eta)$ and $H'''(\eta)$ for the first, third, and fifth two-dimensional similarity solutions (lines) together with results from the time-dependent simulations (circles). Each successive similarity solution has an extra half-oscillation in $H'''(\eta)$.

VI. DISCUSSION

Both two-dimensional and axisymmetric rupture of a thin liquid film destabilized by van der Waals forces asymptote towards a self-similar regime in which the film thins as $(t_R-t)^{1/5}$ and the characteristic horizontal lengthscale of rupture decreases as $(t_R-t)^{2/5}$, where t_R-t is the time remaining before rupture. The observed scalings indicate that van der Waals forces, surface tension, and viscous stresses are equally significant in the rupturing thin film. Time-dependent simulations show excellent agreement with solutions to the similarity ordinary differential equations. We suggest that the conclusion of Ref. 22, that surface tension is asymptotically negligible when compared with van der Waals forces or viscous stresses, may have been due to problems with numerical resolution. Though the film-rupture problem has been studied here in strictly two-dimensional and axisymmetric geometries, two-dimensional rupture is unstable to perturbations in film thickness along the third direction, as also would be ring rupture. Since the axisymmetric solution is stable to asymmetric perturbations,[26] it seems plausible that the film thickness would then evolve into axisymmetric rupture. Thus thin films destabilized by van der Waals forces will generally rupture at a point.

We conclude with some thoughts on the limits of validity for the self-similar regime described so far. Returning to dimensional variables, the continuum approximation fails when $h_{\min}(t)\approx d^*$. Since the lateral lengthscale $l(t)$ is given by (8) and (11), it follows that $l(t)=h_{\min}^2(t)/d^*$ and that the aspect ratio $l(t)/h_{\min}(t)\sim h_{\min}(t)/d^*$. Thus the long-wavelength approximation used to derive (6) fails at the same time as the continuum approximation. A similar failure criterion applies to the free-slip condition on the film surface, since the neglect of viscous stresses exerted by the external fluid on the film in comparison with the viscous shear stresses experienced within the film itself requires that $\mu_{\text{ext}}\mathbf{u}_H/l\ll\mu\mathbf{u}_H/h_{\min}$, which fails when $h_{\min}/d^*\lesssim\mu_{\text{ext}}/\mu$.

As the film ruptures, the reduced Reynolds number $\rho u h^2/\mu l$ diverges as $(t_R-t)^{3/5}$, so that the effects of inertia are predicted to become significant when the film thins to thickness

$$h_I=\left(\frac{A^{*2}}{12\pi^2\mu\nu\gamma}\right)^{1/3}. \tag{25}$$

However, for typical parameter values, e.g., $A^*=10^{-13}$ erg, $\gamma=20$ dyne cm^{-1}, $\rho=1$ g cm^{-3}, and $\mu=10^{-2}$ g cm^{-1} sec^{-1}, h_I is less than the molecular length-

scale d^*. For typical fluids, then, the neglect of inertia fails after the continuum and long-wavelength approximations. For the theoretical problem in which $h_I \gg d^*$, scaling analysis would appear to allow two possible balances of forces in the subsequent inertial regime, each of which fully determines the time dependence of the film thickness and the horizontal lengthscale. One possibility balances inertia, van der Waals forces, and surface tension, in which case $h \sim (t_R - t)^{2/7}$ and $l \sim (t_R - t)^{4/7}$; the other balances inertia, van der Waals forces, and viscous dissipation, in which case $h \sim (t_R - t)^{1/2}$ and $l \sim (t_R - t)^{1/4}$. In view of the parameter values, we have not investigated this further.

Equation (9) can also describe the thinning, under van der Waals forces, of a less viscous liquid film between two very viscous droplets when the viscosity ratio μ/μ_{droplet} is much smaller than the aspect ratio $h/(ah)^{1/2}$, where a is the drop radius and h is the minimum gap thickness. As $h \to 0$ this inequality must eventually be violated, which makes it of interest to extend analysis of self-similar rupture to the case of arbitrary viscosity ratio. Though there can be a complex interaction between droplet deformation and film thinning during the approach to coalescence,[25,27] the final stages are dominated by van-der-Waals-driven rupture and a knowledge of the asymptotic, self-similar behavior of the thinning gap might be useful in creating better cutoff schemes in coarse-grained simulation of droplet interactions.

Finally, we note that, though the self-similar regime in this rupture problem, like that of other finite-time singularities, spans only the final instants of the rupture process, it is nevertheless significant as the self-similar regime constitutes the limiting regime towards which the nonlinear transient state evolves. Thus a knowledge of the self-similar behavior associated with a finite-time singularity can provide insights into the physical behavior of the system which cannot easily be obtained from either stability analyses or full numerical calculations. The mathematical tools developed in the study of finite-time singularities may also have more general applications in the analysis of nonlinear systems.

ACKNOWLEDGMENTS

We are very grateful to E. J. Hinch for sharing his earlier work on the problem and to H. A. Stone for comments on a draft of this paper. W. W. Zhang is supported by a NSF graduate research fellowship and also acknowledges partial support from Harvard University's Materials Research Science and Engineering Center (grant to H. A. Stone).

APPENDIX: NUMERICAL SCHEMES FOR TIME-DEPENDENT SIMULATIONS

The anticipation that the film profile asymptotes towards a similarity solution whose horizontal length scales as the square of minimum film thickness motivated the variable transformation,

$$r(s) = h_{\min}^2(t) \sinh(s), \tag{A1}$$

in the axisymmetric problem and an analogous transformation of x in the two-dimensional problem. Here r is the radial coordinate in the axisymmetric problem, and x is the horizontal coordinate in the two-dimensional problem; $s(r,t)$ is the coordinate used in the numerical scheme. The grid-point distribution was uniform in s so that the grid spacing in r was nearly uniform near the origin but increased proportional to r away from the origin. The variable transformation is consistent with the symmetry of the boundary conditions at the origin.

Each time step was made using the current (fixed) grid, implicit representation of the higher derivatives in each term of (9), and the current value of the nonlinear coefficients. After each time step, a new grid was defined from the new value of $h_{\min}(t)$ and additional grid points were introduced to keep the grid spacing in s roughly constant. Values of $h(r,t)$ at the new set of grid points were obtained from the original set by cubic interpolation. The time step Δt was chosen by

$$\Delta t = \frac{\Delta r^4}{h_{\min}^3(t)} \approx h_{\min}^5(t) \Delta s^4, \tag{A2}$$

where Δr is the grid spacing near the origin. This choice of time step ensures that evolution on grid scales near the origin is followed throughout the rupture process. The variable transformation (A1) leaves features away from the origin under-resolved spatially for the time step (A2). However, since the far-field free-surface profile is almost quasi-steady, the error is expected to be small and not to influence the region of self-similar rupture. To test this expectation, the axisymmetric rupture simulation was repeated with a different transformation,

$$r(s) = h_{\min}^2(t) s\left(\frac{s^2 + (s^4+4)^{1/2}}{2}\right)^{1/2}, \tag{A3}$$

where again the point distribution is uniform in s. The grid spacing in r is still nearly uniform near the origin but increases as $r^{1/2}$, instead of r, away from the origin. This choice is motivated by the $r^{1/2}$ intermediate asymptotic scaling (Fig. 4), and uses many more grid points in the far field. Comparison of simulations using (A3) with simulations using (A1) and the same spatial resolution near the origin showed no significant difference either in the self-similar behavior or the approach to self-similarity. We expect the same to be true for two-dimensional rupture. All results presented here are therefore from simulations which used the cheaper scheme (A1).

The values of $H(0)$, $H''(0)$, and A in each geometry are deduced from two simulations with the same initial condition but different grid spacings. For example, the axisymmetric values were obtained from two runs, one of which began with 16 data points increasing to 306 by $h_{\min}(t) = 10^{-10}$, while the other began with 48 data points increasing to 919 by $h_{\min}(t) = 10^{-10}$. Error estimates for $H(0)$, $H''(0)$, and A can be obtained by comparison of the results from the two runs.

[1] J. Eggers, ''Universal pinching of 3D axisymmetric free-surface flow,'' Phys. Rev. Lett. **71**, 3458 (1993).
[2] D. T. Papageorgiou, ''On the breakup of viscous fluid jets,'' Phys. Fluids **7**, 1529 (1995).
[3] M. P. Brenner, J. R. Lister, and H. A. Stone, ''Pinching threads, singularities and the number 0.0304...,'' Phys. Fluids **8**, 2827 (1996).

[4]R. F. Day, E. J. Hinch, and J. R. Lister, ''Self-similar capillary pinchoff of an inviscid fluid,'' Phys. Rev. Lett. **80**, 704 (1998).
[5]J. R. Lister and H. A. Stone, ''Capillary breakup of a viscous thread surrounded by another viscous fluid,'' Phys. Fluids **10**, 2758 (1998).
[6]J. Eggers, ''Nonlinear dynamics and breakup of free-surface flows,'' Rev. Mod. Phys. **69**(3), 865 (1997).
[7]M. P. Ida and M. J. Miksis, ''Thin film rupture,'' Appl. Math. Lett. **9**(3), 35 (1996).
[8]D. Vaynblat, M. P. Brenner, J. R. Lister, and T. P. Witelski, ''Points, sheets, and threads: dimensionality dependence of droplet fission'' (in preparation).
[9]P. Constantin, T. F. Dupont, R. E. Goldstein, R. E. Kadanoff, M. J. Shelley, and S. M. Zhou, ''Droplet breakup in a model of the Hele-Shaw cell,'' Phys. Rev. E **47**, 4169 (1993).
[10]T. F. Dupont, R. E. Goldstein, L. P. Kadanoff, and S. M. Zhou, ''Finite-time singularity in Hele-Shaw systems,'' Phys. Rev. E **47**, 4182 (1993).
[11]R. E. Goldstein, A. I. Pesci, and M. J. Shelley, ''Topology transitions and singularities in viscous flows,'' Phys. Rev. Lett. **70**, 3043 (1993).
[12]R. Almgren, A. L. Bertozzi, and M. P. Brenner, ''Stable and unstable singularities in the unforced Hele-Shaw cell,'' Phys. Fluids **8**, 1356 (1996).
[13]R. E. Pattle, ''Diffusion from an instantaneous point source with a concentration-dependent coefficient,'' Q. J. Mech. Appl. Math. **12**, 407 (1959).
[14]A. L. Bertozzi, M. P. Brenner, T. F. Dupont, and L. P. Kadanoff, ''Singularities and similarities in interface flows,'' in *Trends and Perspectives in Applied Mathematics*, edited by L. Sirovich (Springer, New York, 1993), p. 155.
[15]A. L. Bertozzi, ''Symmetric singularity formation in lubrication-type equations for interface motion,'' SIAM (Soc. Ind. Appl. Math.) J. Appl. Math. **56**, 681 (1996).
[16]A. L. Bertozzi and M. Pugh, ''The lubrication approximation for thin viscous films: Regularity and long-time behaviour of weak solutions,'' Commun. Pure Appl. Math. **49**, 85 (1996).
[17]A. L. Bertozzi and M. Pugh, ''The lubrication approximation for thin viscous films: the moving contact line with a porous media cut-off of van der Waals interactions,'' Nonlinearity **7**, 1535 (1994).
[18]A. L. Bertozzi and M. Pugh, ''Long-wave instabilities and saturation in thin film equations,'' Commun. Pure Appl. Math. **51**, 625 (1998).
[19]A. J. Bernoff, A. L. Bertozzi, and T. P. Witelski, ''Axisymmetric surface diffusion: Dynamics and stability of self-similar pinch-off,'' J. Stat. Phys. **93**, 725 (1998).
[20]H. Wong, M. J. Miksis, P. W. Voorhees, and S. H. Davis, ''Universal pinchoff of rods by capillarity-driven surface tension,'' Scr. Mater. **39**, 55 (1998).
[21]M. B. Williams and S. H. Davis, ''Nonlinear theory of film rupture,'' J. Colloid Interface Sci. **90**, 220 (1982).
[22]J. P. Burelbach, S. G. Bankoff, and S. H. Davis, ''Nonlinear stability of evaporating/condensing liquid films,'' J. Fluid Mech. **195**, 463 (1988).
[23]A. Oron, S. H. Davis, and S. G. Bankoff, ''Long-scale evolution of thin liquid films,'' Rev. Mod. Phys. **69**(3), 931 (1997).
[24]D. Tabor, *Gases, Liquids and Solids and Other States of Matter* (Cambridge U. P., Cambridge, 1991).
[25]S. G. Yiantsios and R. H. Davis, ''On the buoyancy-driven motion of a drop towards a rigid surface or a deformable interface,'' J. Fluid Mech. **217**, 547 (1990).
[26]T. P. Witelski and A. J. Bernoff, ''Stability of self-similar solutions for van der Waals driven thin film rupture,'' Phys. Fluids **11**, 2443 (1999).
[27]S. G. Yiantsios and R. H. Davis, ''Close approach and deformation of two viscous drops due to gravity and van der Waals forces,'' J. Colloid Interface Sci. **144**, 412 (1991).